ELECTRIC FIELD EFFECTS ON TRAVELLING WAVES IN THE OREGONATOR MODEL FOR THE BELOUSOV–ZHABOTINSKY REACTION

by I. KISS, J. H. MERKIN

(*Department of Applied Mathematics, University of Leeds, Leeds* LS2 9JT)

S. K. SCOTT

(*Department of Chemistry, University of Leeds, Leeds* LS2 9JT)

and P. L. SIMON

(*Department of Applied Analysis, Eötvös University, Budapest, Hungary*)

[Received 26 January 2004. Revise 13 June 2004. Accepted 15 June 2004]

Summary

The effects of an electric field on the travelling waves arising in Belousov–Zhabotinsky systems are analysed using the Oregonator to describe the kinetics. The model is reduced to a two-variable version involving the concentrations of $HBrO_2$ and M_{ox}^{3+}, the oxidized form of the catalyst, using previously-suggested scalings. The travelling wave equations for this two-variable model are solved numerically for a range of kinetic parameters and the ratio of diffusion coefficients D. An upper bound on the field strength E is found, arising from a saddle-node bifurcation, for the existence of travelling waves. There can also be a lower bound on E for their existence, dependent on the other parameters in the system. The conditions for this termination of a solution at a finite field strength are determined. In other cases, travelling waves exist for all negative field strengths and an asymptotic solution for large $|E|$ is constructed. This acts as a confirmation of the numerical results and provides further insights into the structure of the wave profiles. Numerical integrations of the corresponding initial-value problem are undertaken. These show wave deceleration and annihilation in positive fields and wave acceleration in negative fields, in line with experimental observations. In cases when there is termination at a finite value of E, wave trains are seen to develop for (negative) field strength less than this value.

1. Introduction

Propagating pulses of reaction are usually well-ordered structures and, as such, play an important role in many chemical and biological processes. They often arise in excitable media, whereby the system undergoes a rapid reaction, the 'excitory region', followed by a slow recovery to its original state. During this latter process the system is refractory, insensitive to further stimuli and needs to have returned sufficiently close to its rest state before further waves can be generated. As a consequence, excitable media subject to external stimuli usually form either individual waves or regular trains of equally spaced waves. The excitable media studied in most detail, both

experimentally and theoretically, are, perhaps, systems based on the Belousov–Zhabotinsky (BZ) reaction. This system is often used as a paradigm for the more complex excitable media that arise in biological applications. This reaction exhibits all the features particular to excitable media, single reaction pulses and wave trains in 1D and, in 2D, target patterns and spirals (forming under suitable conditions).

When an electric field is applied to a BZ system the resulting behaviour can become much more complex. In 1D wave acceleration and deceleration as well as wave annihilation are observed (**1** to **3**), though, perhaps the most unexpected behaviour seen in 1D is wave splitting. In this a sequence of waves become detached from the rear of the original wave and travel in a direction opposite to that of the original wave. In 2D an initially symmetric, radially spreading wave can be broken when an electric field of sufficient strength is applied, with spirals forming at the broken ends (**4** to **6**). There is also the possibility of more waves forming at these broken ends (perhaps the analogue of wave splitting seen in 1D). As the reaction proceeds under the influence of the electric field, further wave breakings and recombinations can arise, depending on the electric field strength and the specific chemical composition of the reactant mixture. Applying direct or alternating electric fields to BZ systems has also been observed (**7** to **12**) to cause complex motion of spiral centres in 2D configurations.

Models for BZ systems are usually based on Oregonator kinetics (**13**, **14**), which involves the three active species, an autocatalyst $HBrO_2$, an inhibitor Br^- and an oxidised form of the catalyst M_{ox}^{3+} (usually ferriin). Expressing this mechanism in dimensionless form (**15** to **17**) shows that, to a good approximation, the concentration of Br^- can be regarded as varying quasi-statically in relation to the concentrations of the other two active species. In this reduced, two-variable form, the reaction dynamics are relatively simple. There is only one (chemically acceptable) steady state, with parameter values for which this is an excitable state. There is also the possibility of oscillatory behaviour arising from Hopf bifurcations. This two-variable reaction mechanism has been used extensively as the kinetics in models of spatially-distributed systems, both as a generic model for excitable media and, more directly, to describe specific effects seen in BZ systems (effects of electric fields and differential illumination on a light sensitive version of the BZ reaction are two such examples). The consequences of making the reduction from the three-variable to the two-variable system on the travelling waves are examined briefly in the field-free case, where perhaps larger than expected differences between the two waveforms are seen.

More detailed kinetics have been suggested for modelling the BZ reaction, a review and a detailed examination of some of these different mechanisms is given in (**4**). These mechanisms involve further active species and further kinetic steps and are thought to provide a better description for BZ chemistry. The reaction dynamics of these extended schemes can be much more complex than for the two-variable Oregonator, multistability and further bifurcations can arise. This makes models based on these extended schemes as the kinetics in spatially-distributed systems more difficult to analyse, as the nature of their 'base state' is not readily determined. This can, in turn, make it difficult to unravel the mechanisms that lead to structures that are essentially spatially-distributed.

Thus there are advantages to using two-variable Oregonator kinetics in trying to understand how propagating waves and other spatio-temporal structures arise, both as a model for a general excitable system and for specific BZ systems. This is the purpose of our paper. In particular, we develop a spatially-distributed model for a BZ system which includes the effects of applying electric fields to the reactants and which uses the Oregonator model for the kinetics. We make our basic reaction–diffusion electromigration model dimensionless using the standard scalings used previously (**15** to **17**). We show, to be consistent with previous studies, that Br^- should still be regarded as in a

quasi-steady state. This reduces our model to one for the two variables, $HBrO_2$ and M_{ox}^{3+}, and we examine this reduced model in detail. Our main aim is to determine the range of behaviour that our model can predict that is also observed experimentally and to see if there are any features seen in the experiments which are not also supported by our model. This will allow an assessment to be made of the viability of using two-variable Oregonator kinetics for modelling electric field effects on BZ systems. This kinetic model (in its reduced form) has proved effective in explaining the nature of flow-driven structures in BZ systems (see (**18** to **20**), for example) and in wave and spiral modifications in light sensitive media ((**21** to **23**) provide examples).

Previous studies have highlighted the subtle nature of the interaction of an applied electric field with reacting and diffusing ionic chemical species. The initial work by Schmidt and Ortoleva (**24** to **26**) and Ortoleva (**27**) showed that electric fields can have a considerable influence on wave propagation and pattern formation in chemical systems. Later studies of reaction fronts in autocatalytic systems (**28** to **30**) have shown a much greater range of complex behaviour than might have been expected in these simple systems. Much of this was seen in a detailed examination, both experimentally and theoretically, of reaction fronts in the iodate–arsenous acid system subjected to applied electrc fields (**31**, **32**). Models based on two-variable Oregonator kinetics for the effects of electric fields on BZ systems have been studied previously. However, these tend to be inconsistent with the ionic charges of the reactants, usually assuming that there is electromigration of $HBrO_2$ caused by the electric field, (**12**, **33**) for example. Although these models can be regarded as good generic models for convective (electromigratory) effects on excitable media, they have drawbacks when applied specifically to interpreting the behaviour of a BZ system.

2. Model

Oregonator kinetics for the BZ reaction can be conveniently expressed as

$$\begin{aligned} A + Y &\to X + P \quad \text{rate } k_3 a y, \\ X + Y &\to 2P \quad \text{rate } k_2 x y, \\ A + X &\to 2X + 2Z \quad \text{rate } k_5 a x, \\ 2X &\to A + P \quad \text{rate } k_4 x^2, \\ B + Z &\to \frac{1}{2} f Y \quad \text{rate } k_c b z, \end{aligned} \tag{1}$$

where $X \equiv [HBrO_2]$, $Y \equiv [Br^-]$ and $Z \equiv [M_{ox}^{3+}]$ are the active species. We treat $A \equiv [BrO_3^-]$ and B (representing all oxidised organic species) as pooled chemicals, that is, they are assumed to remain at their initial concentrations throughout. As P represents reaction products it does not enter our discussion. The dependence of the reaction rates on $[H^+]$ in (1) has been omitted as we are assuming that the system is run at constant pH (which is usually the case in experiments).

To derive the reaction–diffusion electromigration equations governing our system, we make the constant field approximation. This is valid provided that the other, non–reacting ionic species are in plentiful supply compared to the reacting ionic species Br^- and M_{ox}^{3+} (**34**). We take planar geometry using x and t as our space and time variables. This leads to the equations, on using (1),

$$\frac{\partial X}{\partial t} = D_X \frac{\partial^2 X}{\partial x^2} + k_3 A Y - k_2 X Y + k_5 A X - 2k_4 X^2, \tag{2}$$

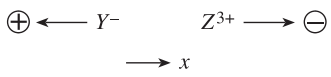

Fig. 1 Electromigratory effect on Y^- and Z^{3+} of applying an electric field $\mathcal{E} > 0$

$$\frac{\partial Y}{\partial t} = D_Y \frac{\partial^2 Y}{\partial x^2} + D_Y \mathcal{E} \frac{\partial Y}{\partial x} - k_3 AY - k_2 XY + \frac{1}{2} f k_c B Z, \tag{3}$$

$$\frac{\partial Z}{\partial t} = D_Z \frac{\partial^2 Z}{\partial x^2} - 3 D_Z \mathcal{E} \frac{\partial Z}{\partial x} + 2 k_5 AX - k_c B Z, \tag{4}$$

where D_X, D_Y and D_Z are the diffusion coefficients of reactants X, Y^- and Z^{3+} respectively and $\mathcal{E}$ is a measure of the (constant) applied electric field strength. The additional migratory effect of applying the electric field ($\mathcal{E} > 0$) on the ionic species Y^- and Z^{3+} is shown in Fig. 1.

We make (2) to (4) dimensionless using the scalings suggested originally by Tyson (**15** to **17**), namely

$$X = \left(\frac{k_5 A}{2k_4}\right) u, \quad Y = \left(\frac{k_5 A}{k_2}\right) v, \quad Z = \left(\frac{(k_5 A)^2}{k_4 k_c B}\right) w, \quad \bar{t} = (k_c B) t, \quad \bar{x} = x \left(\frac{k_c B}{D_X}\right)^{1/2}. \tag{5}$$

Applying (5) in (2) to (4) and dropping the bars on the dimensionless time and space variables $\bar{t}$, $\bar{x}$ for convenience, we obtain the dimensionless system

$$\frac{\partial u}{\partial t} = \frac{\partial^2 u}{\partial x^2} + \frac{1}{\epsilon} \left(u(1-u) - uv + qv\right), \tag{6}$$

$$\frac{\partial w}{\partial t} = D_W \frac{\partial^2 w}{\partial x^2} - D_W E \frac{\partial w}{\partial x} + u - w, \tag{7}$$

$$\epsilon' \left(\frac{\partial v}{\partial t} - D_V \frac{\partial^2 v}{\partial x^2} - \frac{1}{3} D_V E \frac{\partial v}{\partial x}\right) = f w - (q + u) v, \tag{8}$$

where

$$q = \frac{2k_3 k_4}{k_2 k_5}, \quad \epsilon = \frac{k_c B}{k_5 A}, \quad \epsilon' = \frac{2k_c k_4 B}{k_2 k_5 A} \tag{9}$$

are the usual kinetic parameters and where

$$D_W = \frac{D_Z}{D_X}, \quad D_V = \frac{D_Y}{D_X}, \quad E = 3\mathcal{E} \left(\frac{D_X}{k_c B}\right)^{1/2}. \tag{10}$$

We note that the choice of dimensionless variables (5), which preserves the essential form of the

original dimensionless version of the Oregonator model, forces the parameter ϵ' to multiply both the diffusion and electromigration terms in equation (8) for Br^-. The reduced model is then derived on the assumption that $\epsilon' \ll 1$, it is usually at least an order of magnitude less than ϵ. Then formally letting $\epsilon' \to 0$ in equation (8) shows that v is in the quasi-steady state

$$v = \frac{fw}{u+q}. \tag{11}$$

On using (11) in (6), (7) we obtain our reduced model as

$$\frac{\partial u}{\partial t} = \frac{\partial^2 u}{\partial x^2} + \frac{1}{\epsilon}\left(u(1-u) - \frac{fw(u-q)}{(u+q)}\right), \tag{12}$$

$$\frac{\partial w}{\partial t} = D\frac{\partial^2 w}{\partial x^2} - DE\frac{\partial w}{\partial x} + u - w \tag{13}$$

for u and w which are dimensionless versions of $[HBrO_2]$ and $[M^{3+}_{ox}]$ respectively and where we have replaced D_W by D.

Note that, in this reduction, the electric field appears only in the equation for $[M^{3+}_{ox}]$, the only ionic species in this version. It is the model given by (12), (13) that we now consider in detail. Before doing so we give a brief description of the spatially uniform system.

2.1 *Spatially uniform system*

This system is given by the ordinary differential equations that are obtained from (12), (13) with the spatial derivatives omitted. This has the single steady state

$$u_s = w_s = \tfrac{1}{2}\left(1 - (f+q) + \sqrt{(1-f-q)^2 + 4q(1+f)}\right). \tag{14}$$

The (linear) stability of this steady state is determined by putting

$$u = u_s + U, \quad w = w_s + W, \qquad \text{where } U, W \ll 1. \tag{15}$$

This results in the linear equations

$$\dot{U} = \frac{1}{\epsilon}(\alpha U - \beta W), \qquad \dot{W} = U - W, \tag{16}$$

where

$$\alpha = 1 - 2u_s - \frac{2fqu_s}{(u_s+q)^2}, \qquad \beta = \frac{f(u_s - q)}{(u_s+q)}. \tag{17}$$

Note that $\beta > 0$ and $\beta - \alpha > 0$.

Equations (16) show that the steady state (14) is stable $\alpha < \epsilon$, with there being a Hopf bifurcation when $\alpha = \epsilon$. The situation is illustrated in Fig. 2 with plots of α against f for representative values of q. The Hopf bifurcations occur when the line $\alpha = \epsilon$ intersects the appropriate curve. It can do so at two values of f, f_1 and f_2 say, for a given value of q. The system is oscillatory for f in the range $f_1 < f < f_2$ and is an excitable system for $f > f_2$. The nature of the Hopf bifurcation is easily determined by BIFOR2 (**35**). Our calculations for a range of values of q show that this bifurcation is subcritical at the smaller value of f and supercritical for the larger value. For example, for $q = 0{\cdot}002$ the Hopf bifurcation is degenerate at $\epsilon = \epsilon^* = 0{\cdot}8006$, $f = f^* = 0{\cdot}9760$, changing from subcritical for $f < f^*$ to supercritical for $f > f^*$.

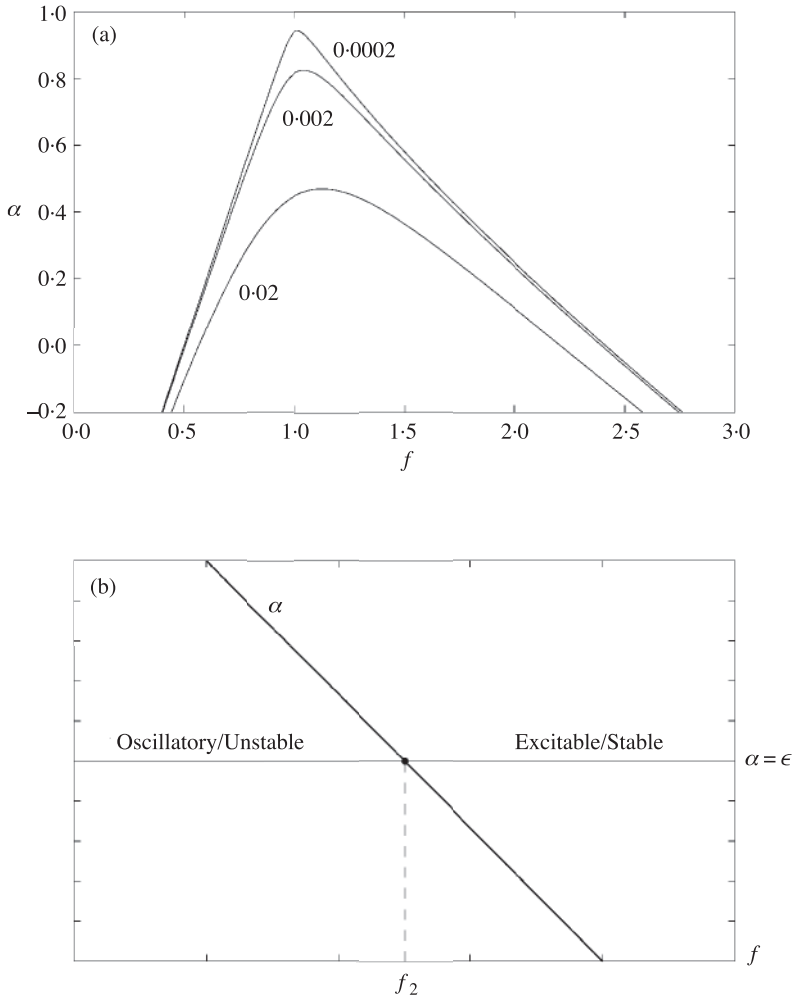

Fig. 2 (a) Plots of α, as defined in (17), against f for $q = 0{\cdot}02,\ 0{\cdot}002,\ 0{\cdot}0002$. The spatially uniform system is stable for $\alpha < \epsilon$. (b) A sketch of α against f to show the change from unstable (oscillatory) to stable (excitable) behaviour at $f = f_2$ when $\alpha = \epsilon$

3. Spatially distributed system

3.1 *Travelling waves*

We start by considering the travelling waves (single pulses) that can arise in our model (12), (13). To derive the travelling wave equations we introduce the travelling coordinate $y = x - ct$, where c is the (constant) wave speed and take u and w to depend only on y. This leads to the ordinary

differential equations

$$u'' + cu' + \frac{1}{\epsilon}\left(u(1-u) - \frac{fw(u-q)}{(u+q)}\right) = 0, \tag{18}$$

$$Dw'' + (c - DE)w' + u - w = 0 \tag{19}$$

on $-\infty < y < \infty$ (where primes denote differentiation with respect to y). The boundary conditions are

$$u \to u_s, \quad w \to w_s \quad \text{as } |y| \to \infty, \tag{20}$$

where u_s and w_s are given by (14).

We were able to solve (18) to (20) numerically using the method described in (**37**). These numerical solutions calculate the wave speed c for given values of the parameters and are continued in one of the parameters using a pseudoarclength method. In Fig. 3a we give plots of c against the electric field strength E for $f = 2{\cdot}5$ and $D = 1{\cdot}0$, $q = 0{\cdot}002$ and for a range of values of ϵ (noted on the figure). All the curves have a similar characteristic in that they show a saddle-node bifurcation at $E = E_m$, with two solution branches for $E < E_m$. For the smaller values of ϵ there is a local minimum for c on the lower solution branch. Both solution branches are unbounded for negative values of E (at least as far as we have been able to compute) and on the upper solution branch c appears to be tending to a constant value (dependent on ϵ) as $E \to -\infty$. For the larger values of ϵ, $E_m < 0$ with the case when $E_m = 0$ being determined from (**37**) at $\epsilon = \epsilon_0 = 0{\cdot}076$. For values of $\epsilon > \epsilon_0$ there are no travelling waves in positive fields for this value of f.

We are able to compute the limiting field strength E_m using the method developed in (**37**) and a graph of E_m against ϵ is shown in Fig. 3b (for the same parameter values as before). The change in sign of E_m at ϵ_0 is clearly seen in the figure with E_m increasing monotonically as ϵ is decreased. For larger values of ϵ travelling waves are possible only in strong negative fields, for example, at $\epsilon = 0{\cdot}5$, $E_m = -5{\cdot}3991$. This figure also shows that, when the system is in its more excitable state—small values of ϵ—small changes in the electric field strength can radically affect whether waves propagate or fail in positive fields.

The effect of the electric field is to alter the wave profile. This is illustrated in Fig. 4 with plots of u and w profiles for a range of values of E, with $f = 2{\cdot}35$, $\epsilon = 0{\cdot}05$, $q = 0{\cdot}002$, $D = 1{\cdot}0$. The effect of a positive electric field is to decrease both the height and lateral spread of both the u and w profiles; compare the profiles for $E = 0{\cdot}9$ with those for $E = 0$. A negative field has the opposite effect. The lateral spread of both the u and w profiles and the maximum of the u profile are increased as the value of $|E|$ is increased. The effect on the maximum value of w in the wave is for it to be first increased in the smaller negative fields and then to decrease as the field strength is increased; compare the w profiles for $E = -1{\cdot}0$ and $E = -20{\cdot}0$ in Fig. 4b.

We next consider the effect of the stoichiometry factor f on the solution. We take $\epsilon = 0{\cdot}05$ ($q = 0{\cdot}002$, $D = 1{\cdot}0$) and plot curves of c against E for a range of values of f in Fig. 5a. There is again a maximum value E_m of E for the existence of a travelling wave solution with a saddle-node bifurcation at $E = E_m$. The value of E_m decreases as f is increased and for f greater than about $3{\cdot}2$ we find that $E_m < 0$, as might be expected from Fig. 3a. For the larger values of f (the curves for $f \geqslant 2{\cdot}5$) both solution branches continue to large $|E|$ for negative fields, with the upper branch solutions appearing to tend to a constant value as $E \to -\infty$. However, for smaller values

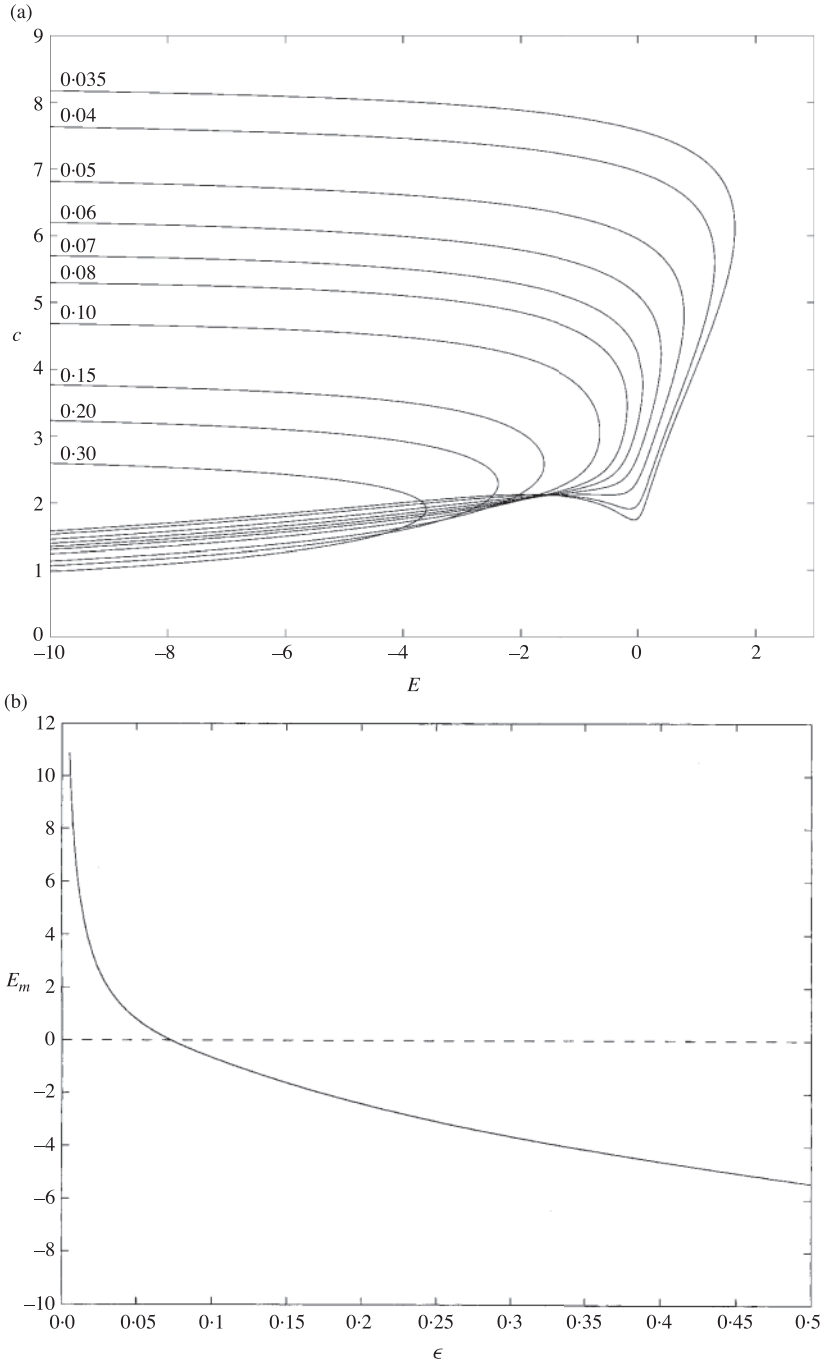

Fig. 3 (a) Plots of the wave speed c of the travelling waves against the electric field strength E for $f = 2{\cdot}5$ and a range of values of ϵ. (b) The electric field strength E_m at the saddle-node bifurcation plotted against ϵ for $f = 2{\cdot}5$. The values of the other parameters are $q = 0{\cdot}002$ and $D = 1{\cdot}0$

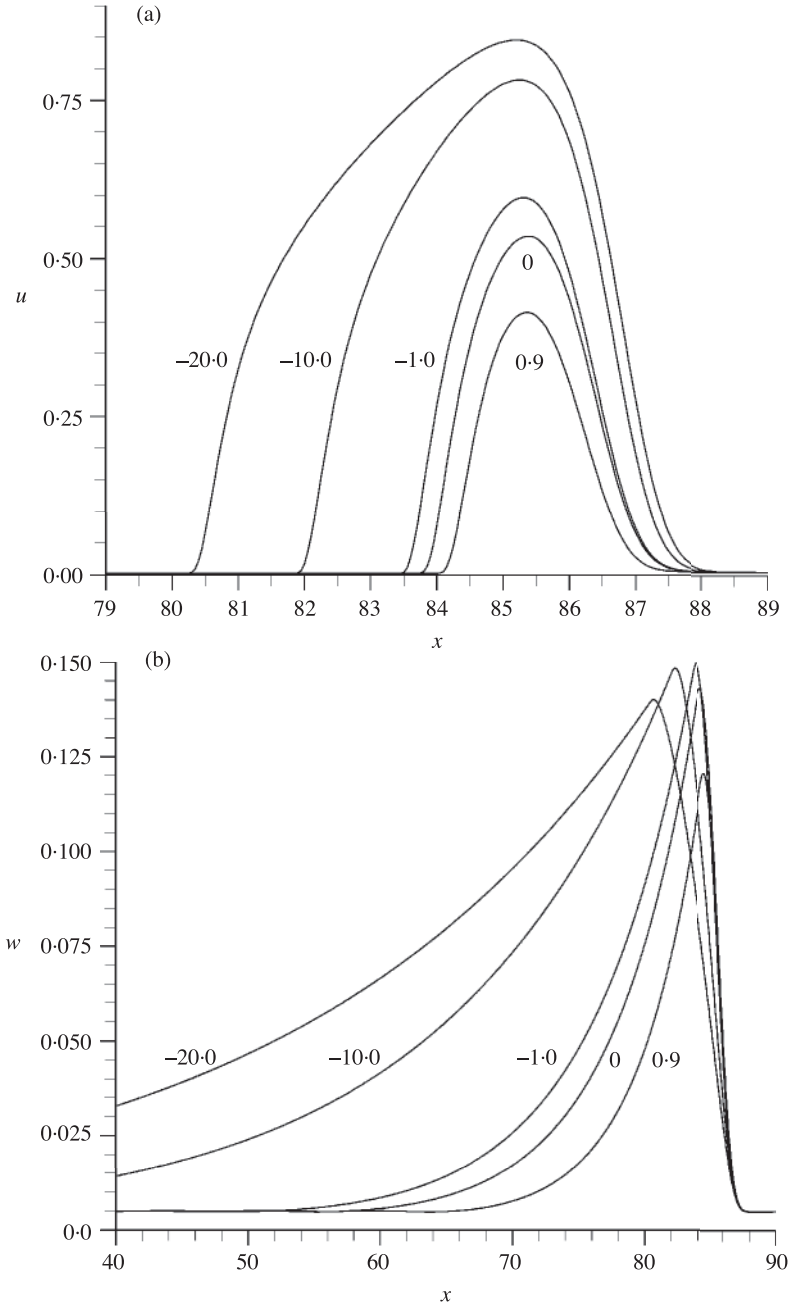

Fig. 4 Plots of the (a) u and (b) w wave profiles for a range of values of E and $f = 2{\cdot}35,\ \epsilon = 0{\cdot}05,\ q = 0{\cdot}002,\ D = 1{\cdot}0$

of f (the curves for $f = 2{\cdot}3,\ 2{\cdot}25$) the solution terminates at a finite value of E. The reason for this is explained in (**37**) and concerns the nature of the eigenvalues λ of the linear equations which approximate the travelling wave equations (18), (19) as $|y| \to \infty$. Considering these equations as a four-dimensional first-order ordinary differential equation and linearizing about the steady state $(u_s, 0, w_s, 0)$ gives the characteristic polynomial for the Jacobian as

$$D\lambda^4 + (c(1+D) - DE)\,\lambda^3 + \left(c(c-DE) + \frac{D\alpha}{\epsilon} - 1\right)\lambda^2 + \left(\frac{\alpha}{\epsilon}(c-DE) - c\right)\lambda + \frac{(\beta-\alpha)}{\epsilon} = 0. \tag{21}$$

A travelling wave (pulse) is a solution of equations (18), (19) in (u, u', w, w') phase space corresponding to a homoclinic orbit on the steady state $(u_s, 0, w_s, 0)$. A necessary condition for the existence of a homoclinic orbit is that there must be both a stable and an unstable manifold on the steady state. Hence a sufficient condition for the non-existence of a travelling wave is that all the roots of equation (21) have either positive or negative real parts.

For negative fields and for all the cases we computed for positive fields, $(c - DE) > 0$ and so the coefficient of λ^3 in equation (21) is positive. This means that there must be at least one negative real root or two complex conjugate roots with a negative real part. Thus travelling waves (single pulses) fail to exist when equation (21) does not have any roots with a positive real part. Conditions for this to happen can be derived from the Routh–Hurwitz criterion (see (**36**, Appendix 2) for example), which gives a relation between c and E (for given values of the other parameters). These curves are plotted in Fig. 5b for a range of f, together with the wave speed curves for $f = 2{\cdot}3$ and $2{\cdot}25$. This figure shows that, even though the wave speed curves are close together, they end at noticeably different values of E, at respectively $E = -3{\cdot}631$ and $E = -0{\cdot}616$ for the upper branch solutions. This behaviour continues as we decrease f, the wave speed curves change only slightly whereas the 'non-existence' curves have a much greater variation. We find that there is a value of f at which the 'non-existence' curve intersects the wave speed curve at the saddle-node point, occurring at $f = 2{\cdot}115$ for Fig. 5b. For values of f less than this there are only the lower branch solutions. There is then a value for f, just below $f = 1{\cdot}9$ in Fig. 5b, where the 'non-existence' curve lies wholly to the right of any possible wave speed curves and there no travelling waves (as single pulses) for any value of E.

We can gain further information about this wave termination process by considering the solution of equation (21) for negative fields as $|E| \to \infty$, assuming that c remains of $O(1)$ (and positive) in this limit. A standard perturbation approach shows that there are two solutions of $O(1)$, one of $O(|E|)$ and one of $O(|E|^{-1})$. The $O(1)$ solutions are, to leading order, given by

$$\lambda^2 + c\lambda + \alpha/\epsilon = 0. \tag{22}$$

If $\alpha > 0$, then both roots of (22) are negative or have negative real part and, if $\alpha < 0$, they are real and of opposite sign. The other solutions are

$$\lambda \sim -|E|\left(1 + \frac{c}{D}|E|^{-1} + \cdots\right), \qquad \lambda \sim -\frac{(\beta-\alpha)}{D\alpha}|E|^{-1} + \cdots \quad (\alpha \neq 0). \tag{23}$$

When $\alpha = 0$, this latter root becomes

$$\lambda \sim -\frac{\beta}{\epsilon c}|E|^{-1/2} + \cdots.$$

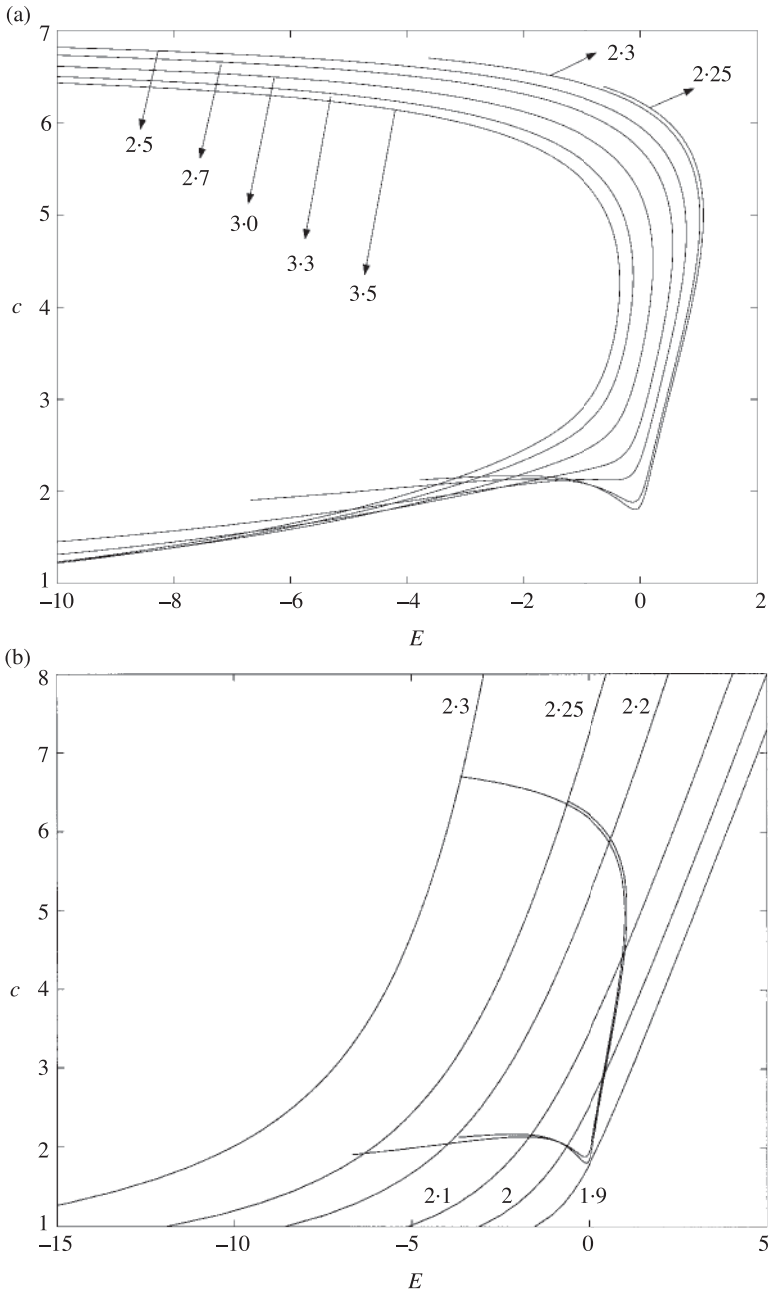

Fig. 5 (a) Plots of the wave speed c of the travelling waves against the electric field strength E for $\epsilon = 0{\cdot}05$ and a range of values of f. (b) 'Non-existence' curves obtained from equation (21) for a range of f and wave speed curves for $f = 2{\cdot}25,\ 2{\cdot}3$, to show the termination of a solution at a finite value of E. For these values of f the kinetic system is unstable. *cont.*

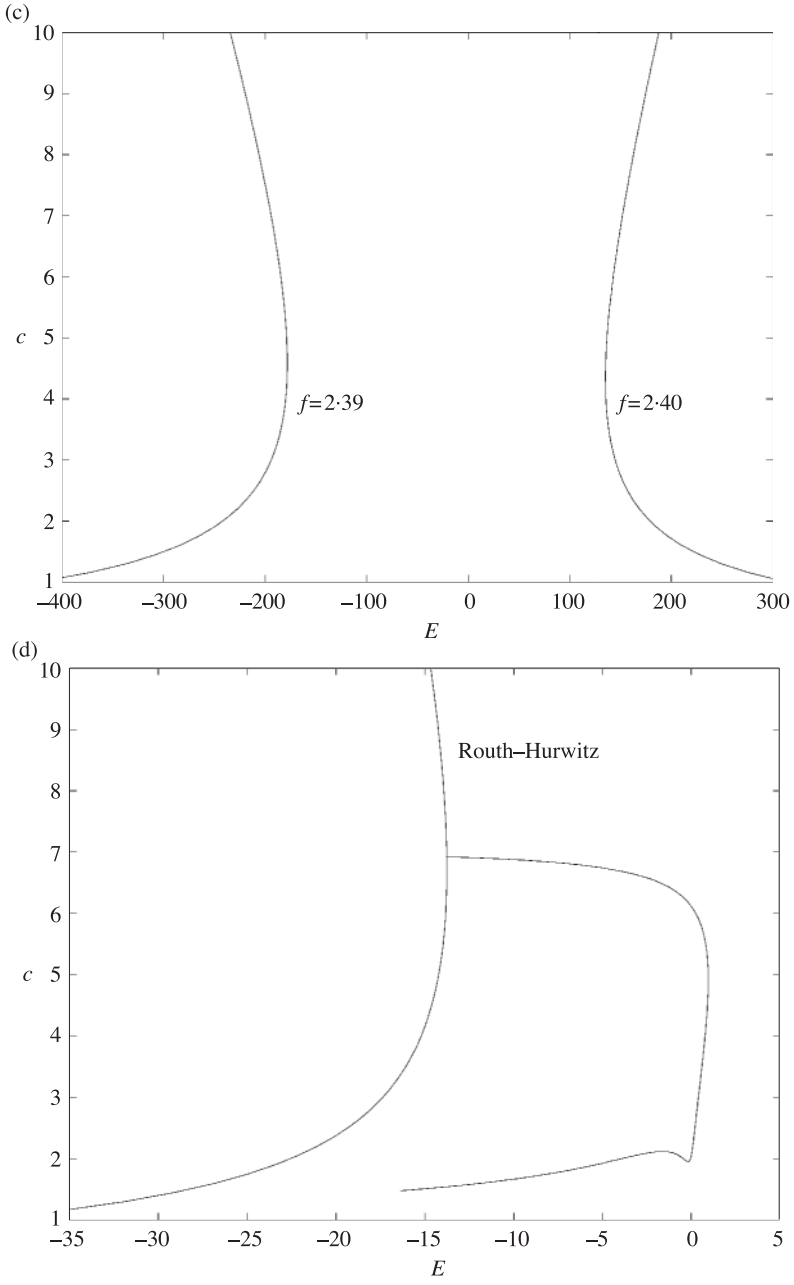

Fig. 5 *cont.* (c) 'Non-existence' curves for $f = 2{\cdot}39$ and $f = 2{\cdot}40$ to, show the transition at $\alpha = 0$. (d) A 'non-existence' curve obtained from the Routh–Hurwitz criteria (RH) and a wave speed plot for $f = 2{\cdot}35$, kinetic system stable. The values of the other parameters are $q = 0{\cdot}002$, $D = 1{\cdot}0$

Expressions (23) show that there is always at least one negative root for $|E|$ large, and with (22) that, if $\alpha > 0$, all roots have negative real parts. Thus a necessary condition for the existence of a travelling wave in the $|E| \to \infty$ limit is that $\alpha < 0$. This, in turn, provides an upper bound (at $\alpha = 0$) on f for the termination of wave solutions at a finite value of E. For $q = 0{\cdot}002$, $\alpha = 0$ at $f = 2{\cdot}39425$ (note that the Hopf bifurcation occurs at $f = 2{\cdot}3087$ for $\epsilon = 0{\cdot}05$). This value for f provides a limiting case for the 'non-existence' curves shown in Fig. 5b. To show the transition at $\alpha = 0$ from having wave solutions terminating at a finite (negative) E to having waves for all negative fields, we plot the 'non-existence' curves for $f = 2{\cdot}39$ ($\alpha > 0$) and for $f = 2{\cdot}40$ ($\alpha < 0$) in Fig. 5c. For $f = 2{\cdot}40$ the curve gives (large) positive values for E and, as we have seen, the solutions finish at a saddle-node bifurcation well before these field strengths are reached.

We explored this point a little further by considering values of f for which the kinetic system is stable, that is, $\alpha < \epsilon$. (Note that, for the values of f in Fig. 5b, the kinetic system is unstable, $\alpha > \epsilon$.) We show a wave speed plot and a 'non-existence' curve obtained from the Routh–Hurwitz criteria for $f = 2{\cdot}35$ in Fig. 5d. The upper branch solution terminates on the 'non-existence' curve at $E = -13{\cdot}778$. As a further check we computed the eigenvalues λ from equation (21) as the travelling wave solution progressed along the upper branch and found that, where the positive eigenvalue was lost was the point of intersection of the two curves in the figure. We were unable to continue the lower branch solution to the 'non-existence' curve. On this branch the solution became oscillatory (with complex values for λ) and we found that eventually we were unable to satisfy the boundary conditions. This occurred at $E = -16{\cdot}36$ in Fig. 5d.

In Fig. 5a we identified a saddle-node bifurcation at $E = E_m$ and, as mentioned above, we can calculate this value in terms of f. The results are shown in Fig. 6 (for $\epsilon = 0{\cdot}05$, $q = 0{\cdot}002$, $D = 1{\cdot}0$). The curve starts at $f = 2{\cdot}115$ (where $E_m = 1{\cdot}235$) and decreases monotonically as f is increased, giving negative values for E_m for $f > 3{\cdot}213$, in line with Fig. 5a.

Our previous study (**37**) suggests that changing the parameter q does not make significant changes in the travelling wave solutions, provided it remains small. However, D, the ratio of diffusion coefficients, can play a more important role. From values given in (**4**), $D \simeq 0{\cdot}3$ and to illustrate this point we computed the wave speed plots for $D = 0{\cdot}3$ and a range of values of f (with $q = 0{\cdot}002$, $\epsilon = 0{\cdot}05$). These are shown in Fig. 7a. The curves have a similar form to those shown in Fig. 5a,b, though the values of E_m are considerably greater, for example with $f = 2{\cdot}5$, $E_m = 0{\cdot}7851$ for $D = 1{\cdot}0$ compared to $E_m = 8{\cdot}1420$ for $D = 0{\cdot}3$. The conditions for the change from having the curves continue to large $|E|$ and finishing at a finite value of E is independent of D; see (22), (23). However, the change in the value of E at which this occurs is greater for $D = 0{\cdot}3$; compare the curves for $f = 2{\cdot}3$ and $f = 2{\cdot}25$ in Fig. 7a with those in Fig. 5b. One feature to note about these curves is that, for the smaller values of f, stable (upper branch) travelling wave solutions exist (as single pulses) only in positive fields. The curve for $f = 2{\cdot}25$ in Fig. 7a terminates at $E = 1{\cdot}6383$ on the 'non-existence' curve RH.

In Fig. 7b we plot E_m, the value of E at the saddle-node bifurcation, against D for $f = 2{\cdot}5$ (and $q = 0{\cdot}002$, $\epsilon = 0{\cdot}05$). The figure shows that E_m decreases monotonically with D, becoming negative at $D \simeq 1{\cdot}39$ and changing only slightly as D is increased further. For smaller values of D; E_m increases rapidly as D is decreased. This can be expected from equation (19) as D multiplies the electric field strength E and, in the limit as $D \to 0$, the situation without an electric field and M_{ox}^{3+} immobile is approached.

In Figs 3a and 5a we saw that the wave speed c appeared to be approaching a constant value for large negative fields. We now consider this further by looking at the solution of equations (18), (19) for $E < 0$ in the limit as $|E| \to \infty$.

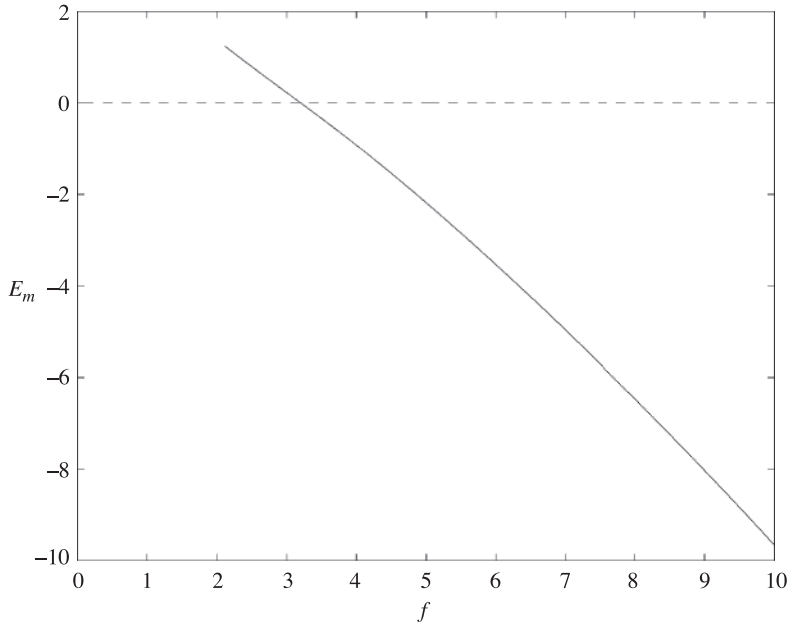

Fig. 6 The electric field strength E_m at the saddle-node bifurcation plotted against f for $\epsilon = 0{\cdot}05$ ($q = 0{\cdot}002,\ D = 1{\cdot}0$)

3.1.1 *Large, negative fields, $E \to -\infty$.* We start our solution at the front of the wave (region I) where we leave the variables unscaled and look for a solution by expanding

$$u(y, |E|) = u_0(y) + u_1(y)|E|^{-1} + \cdots, \quad w(y, |E|) = w_0(y) + w_1(y)|E|^{-1} + \cdots, \quad c(|E|) = c_0 + c_1|E|^{-1} + \cdots. \tag{24}$$

The leading-order problem gives $w_0' = 0$, hence from (20), $w_0 \equiv u_s$, and then

$$u_0'' + c_0 u_0' + \frac{1}{\epsilon}\left(u_0(1-u_0) - \frac{f u_s(u_0 - q)}{(u_0 + q)}\right) = 0, \qquad u \to u_s \ \text{ as } \ y \to \infty. \tag{25}$$

A consideration of equation (25) shows that

$$u_0(y) \to u_a \text{ as } y \to -\infty, \tag{26}$$

where u_a is given by

$$u_a^2 - (1 - q - u_s)u_a + fq = 0, \quad \text{that is, } u_a = \tfrac{1}{2}\left(1 - q - u_s + \sqrt{(1-q-u_s)^2 - 4fq}\right). \tag{27}$$

We note that $u_a > u_s$ at least for the small values of q required by the model.

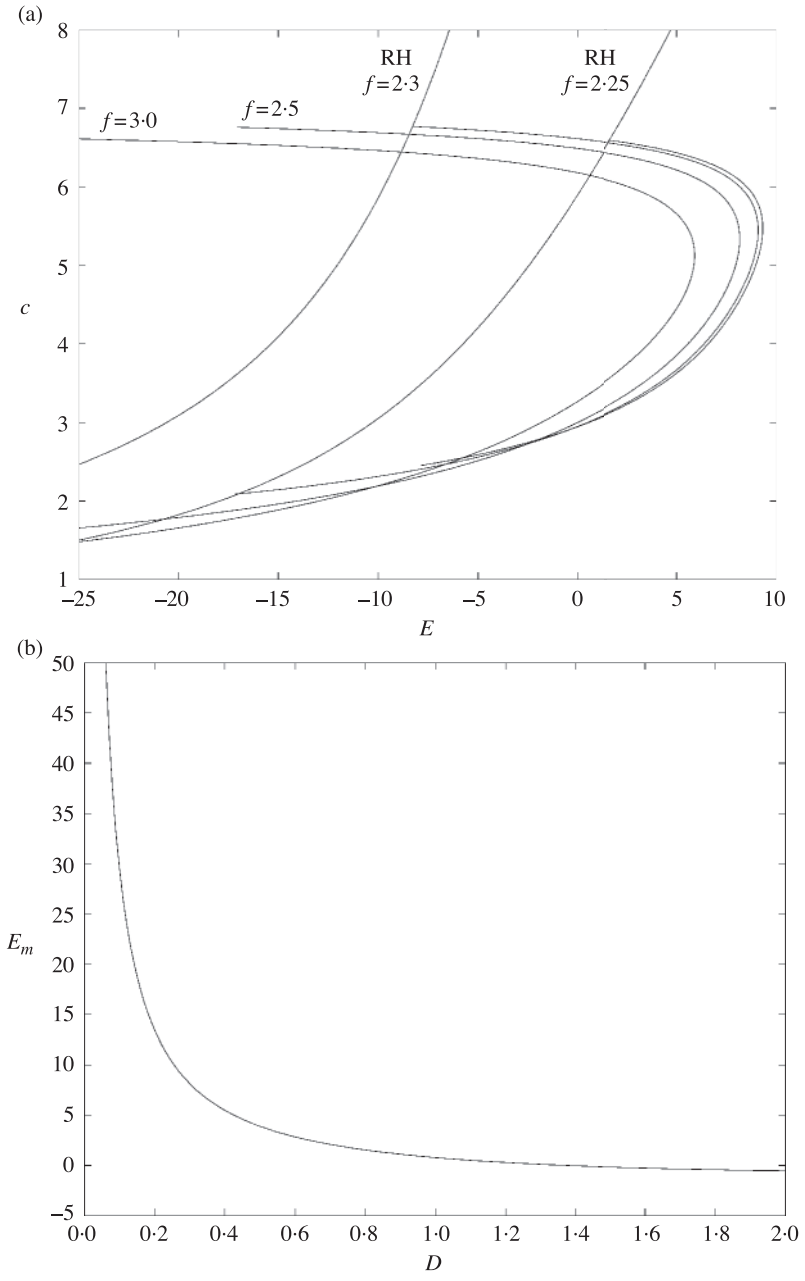

Fig. 7 (a) Plots of the wave speed c of the travelling waves against the electric field strength E for a range of values of f for $D = 0{\cdot}3$. (b) The electric field strength E_m at the saddle-node bifurcation plotted against D for $f = 2{\cdot}5$. The values of the other parameters are $q = 0{\cdot}002$ and $\epsilon = 0{\cdot}05$

To obtain some idea of the values of the various constants that will arise in our discussion it is instructive to evaluate them for small q (note that we take $q = 0{\cdot}002$ in our numerical solutions and that smaller values of q, for example, $q = 0{\cdot}0008$, have also been suggested as reasonable values for this parameter). From (**37**) $u_s \simeq \dfrac{(f+1)}{(f-1)}q$ (for $f > 1$, which is the only case we consider here) and, from (27),

$$u_a \sim 1 - \frac{f(f+1)}{(f-1)}q + \cdots. \tag{28}$$

It is the problem given by (25) to (27) that determines c_0. We can scale ϵ out of this problem by writing $\tilde{y} = \epsilon^{-1/2}y$, $c_0 = \epsilon^{-1/2}\tilde{c_0}$. This reduces the equation to the one that arises in the solution for ϵ small, as discussed in (**37**) where plots of $\tilde{c_0}$ (in the present context) against f for $q = 0{\cdot}002,\ 0{\cdot}0008$ are given. For $q = 0{\cdot}002$ and $f = 2{\cdot}5$, $\tilde{c_0} = 1{\cdot}5651$, giving $c_0 = 1{\cdot}5651\epsilon^{-1/2}$, consistent with the values for large $|E|$ seen in Fig. 3a. In order to obtain a unique value for $\tilde{c_0}$, the equilibrium points $(u_a, 0)$ and $(u_s, 0)$ in the (u, u') phase plane of equation (25) must both be saddle points (giving a saddle–saddle connection). This is the case provided that $\alpha < 0$, as defined by (17), which is precisely the necessary condition derived above for the existence of a travelling wave solution in the large $|E|$ limit.

At $O(|E|^{-1})$, w_1 satisfies $Dw_1' = -(u_0 - u_s)$ from which it follows that $w_1 \sim -(u_a - u_s)y/D$ as $y \to -\infty$. This suggests that the expansion breaks down when y is of $O(|E|)$ and leads to region II, where we put $\overline{y} = |E|^{-1}y$ and still leave u and w unscaled. The leading-order problem for this region is given by

$$u(1-u) - \frac{fw(u-q)}{(u+q)} = 0, \qquad Dw' + u - w = 0 \tag{29}$$

subject to

$$u \sim u_a + \cdots, \qquad w \sim u_s - \left(\frac{u_a - u_s}{D}\right)\overline{y} + \cdots \quad \text{as } \overline{y} \to 0^- \tag{30}$$

on matching with region I. From (29) we obtain

$$\frac{du}{d\overline{y}} = \frac{u(u-u_s)(u+\overline{u}_s)(u-q)}{D(2u^3 - (1+2q)u^2 + 2q(1-q)u + q^2)}, \tag{31}$$

where $-\overline{u}_s$ ($\overline{u}_s > 0$) is the negative root of the quadratic equation that determines the steady state, $\overline{u}_s \sim (f-1)$ for q small. For the values of q that we are concerned with the right-hand side of equation (31) is strictly positive for $u_b < u \leqslant u_a$, where u_b is the largest root of the denominator, with

$$u_b \sim \tfrac{1}{2} - q + \cdots \text{ for } q \text{ small.} \tag{32}$$

Hence there is a value $-\overline{y}_0$ of $\overline{y}$ ($\overline{y}_0 > 0$) at which the solution of equation (31) becomes singular, with $du/d\overline{y} \to \infty$ as $u \to u_b^+$ and

$$u \sim u_b + \sqrt{2A_b}\,(\overline{y} + \overline{y}_0)^{1/2} + \cdots \text{ as } \overline{y} \to -\overline{y}_0, \tag{33}$$

where

$$A_b = \frac{u_b(u_b - u_s)(u_b + \overline{u}_s)(u_b - q)}{2D(3u_b^2 - (1+2q)u_b + q(1-q))}.$$

Since the singularity at $\overline{y} = -\overline{y}_0$ arises from the denominator in equation (29) becoming zero at u_b, which is where $dw/du \to 0$, expression (29) shows that

$$w \sim w_b + B_b(\overline{y} + \overline{y}_0) + \cdots \quad \text{as} \quad \overline{y} \to -\overline{y}_0, \tag{34}$$

where

$$w_b = \frac{u_b(1-u_b)(u_b+q)}{f(u_b - q)}, \quad B_b = -\frac{u_b(u_b-u_s)(u_b+\overline{u}_s)}{Df(u_b-q)} = -\frac{(u_b - w_b)}{D}.$$

Note that

$$A_b \simeq \frac{2f-1}{8D}, \quad w_b \simeq \frac{1}{4f}, \quad B_b \simeq \frac{1-2f}{4Df} \quad \text{for } q \text{ small.}$$

The singularity at $\overline{y} = -\overline{y}_0$ leads to region III where we put

$$\zeta = |E|^{2/3}(\overline{y} + \overline{y}_0), \qquad u = u_b + |E|^{-1/3}U, \qquad w = w_b + |E|^{-2/3}W. \tag{35}$$

The leading-order problem in this region gives

$$D\frac{dW}{d\zeta} = -(u_b - w_b), \quad \text{hence} \quad W = -\left(\frac{u_b - w_b}{D}\right)\zeta \tag{36}$$

on matching with region II, and then after a little algebra

$$\epsilon c_0 \frac{dU}{d\zeta} - \frac{\beta_b}{2A_b}U^2 + \beta_b\zeta = 0, \qquad U \sim \sqrt{2A_b}\,\zeta^{1/2} \quad \text{as} \quad \zeta \to \infty, \tag{37}$$

where $\beta_b = \dfrac{2A_b(3u_b^2 - (1+2q)u_b + q(1-q))}{u_b^2 - q^2}$, with $\beta_b \simeq \dfrac{2f-1}{4D}$ for q small. We can solve equation (37) in terms of Airy functions (**38**) to give, on satisfying the boundary condition,

$$U = -\left(\frac{(2A_b)^2\epsilon c_0}{\beta_b}\right)^{1/3} \frac{\mathrm{Ai}'(\overline{\zeta})}{\mathrm{Ai}(\overline{\zeta})}, \quad \text{where} \quad \overline{\zeta} = \left(\frac{\beta_b^2}{2A_b(\epsilon c_0)^2}\right)^{1/3}\zeta. \tag{38}$$

Expression (38) becomes singular at $\overline{\zeta} = \overline{\zeta}_0$, where $\overline{\zeta}_0$ is the first zero of the Airy function ($\overline{\zeta}_0 = -2{\cdot}3381$), with

$$U \sim -\frac{2A_b\epsilon c_0}{\beta_b(\zeta - \zeta_0)} + \cdots \quad \text{as} \quad \zeta \to \zeta_0. \tag{39}$$

To continue we need a further region, region IV, in which we put $\eta = |E|^{1/3}(\zeta - \zeta_0) = y + |E|\overline{y}_0 - |E|^{1/3}\zeta_0$ and leave u and w unscaled. Thus the equations in region IV are essentially the same as those in region I with now η as independent variable. Following the analysis of region I we

find that now $w \equiv w_b$ to leading order, on matching with region III. This result modifies slightly the leading-order equation for u, which we can now write as

$$u'' + c_0 u' - \frac{(u-u_b)^2}{\epsilon(u+q)}\left(u - \frac{fqw_b}{u_b^2}\right) = 0, \tag{40}$$

where primes denote differentiation with respect to η, subject to the matching condition that

$$u \sim u_b - \frac{2A_b \epsilon c_0}{\beta_b \eta} + \cdots \quad \text{as } \eta \to \infty. \tag{41}$$

A consideration of equation (40) shows that

$$u \to u_c = \frac{fqw_b}{u_b^2} = \frac{q(1-u_b)(u_b+q)}{u_b(u_b-q)} \quad \text{as } \eta \to -\infty, \tag{42}$$

where $u_c \simeq q$ for q small.

To complete the asymptotic expansion we require a final region, region V, where we put $Y = |E|^{-1}\eta$. The equations for this region are, at leading order, essentially the same as in region II, with Y as the independent variable, though now subject to

$$u \to u_c, \quad w \to w_b \quad \text{as } Y \to 0^-. \tag{43}$$

From equation (29) we find that the equation for u is effectively given by (31). Here $u_c < u_s$ (at least for small q) and so the numerator in equation (31) is negative for u in the range $u_c \leqslant u < u_s$. The denominator has a zero at u_b and, for small q, at $u = u_1 \simeq (1 \pm \sqrt{2})q$. Now the condition to have a solution as $|E| \to \infty$ is that $\alpha < 0$, which, for small q, is that $f > 1+\sqrt{2}$ or $u_s < (1+\sqrt{2})q$. Thus under these conditions, u_s is less than the value of u_1, where the denominator of (31) is zero, with the denominator then being positive for $u_c \leqslant u < u_s$. Hence $du/dY < 0$ over this range and equation (31) then shows that $u \to u_s$, $w \to u_s$ as $Y \to -\infty$, the conditions at the rear of the wave. Note that it can readily be shown by direct substitution that having $\alpha = 0$ corresponds to having $(dw/du)_{u_s} = 0$, using the form for $w = w(u)$ given in $(29)_1$.

The above analysis shows the structure of the wave for $|E|$ large (and q small). There is a region (region I) at the front of the wave, of $O(1)$ thickness, where u increases from the small values associated with u_s to a value of approximately unity and w remains unchanged at u_s. It is the solution in this region that fixes the wave speed, which is independent of D in this limit. There is then a wider region (region II), of extent $O(|E|)$, in which the value of u falls to approximately $\frac{1}{2}$ and w increases to its maximum value w_b, of approximately $1/4f$. This region ends in a singularity in the solution for u and to remove this singularity two further regions (regions III and IV), of extent $O(|E|^{1/3})$ and $O(1)$ respectively, are required. In these regions w remains at w_b to leading order. At the end of region IV, u has fallen to a small value of approximately q and it is in the final region, region V, of extent $O(|E|)$, where u increases back to u_s and w approaches u_s from above. The width of the wave is determined mainly by regions II and V, giving an overall extent of $O(|E|)$. Finally we note that the approach to the boundary conditions at both the front and rear of the wave is consistent with that given by (22), (23).

The form of the wave described above is seen in the numerical solutions of the travelling wave equations, the spread of the wave increases with $|E|$ and the maximum values of u and w approach

values of unity and $1/4f$ respectively as $|E|$ is increased (see Fig. 4). As $|E|$ increases the wave speeds approach (finite) limiting values, as given by (25), (26), with these values being independent of D. This can be seen in Figs 3a, 5a and 7a, with values for c for the larger values of $|E|$ being consistent with c_0 calculated from (25), (26), these values are essentially the ones given in (**37**). The result that wave speed is independent of D for $|E|$ large can clearly be seen by comparing the curves for $f = 3{\cdot}0$ and large $|E|$ in Figs 5a ($D = 1$) and 7a ($D = 0{\cdot}3$). The development of the various regions identified in the above asymptotic analysis for large $|E|$ is becoming apparent in the u profile for $E = -20{\cdot}0$ in Fig. 4a.

3.2 *Numerical simulations*

We solved the initial-value problem given by equations (12), (13) using an implicit method based on the Crank–Nicolson scheme with Newton–Raphson iteration to solve the nonlinear finite-difference equations. We started with the system in its spatially uniform steady state (14) and applied a localized perturbation to u, usually putting $u = u_s + 0{\cdot}3$ in a region of width $2{\cdot}0$ centred on $x = 0$. We allowed waves to develop, one propagating in the positive x-direction and one in the negative x-direction, before the electric field was switched on, as suggested by experiments (**4**, **5**). We need treat only positive values of E as the effect of the electric field on a wave propagating in the negative direction is equivalent to taking $-E$. We used a space step $\Delta x = 0{\cdot}05$, the time step Δt was varied to maintain accuracy, usually $\Delta t = 0{\cdot}0032$. The number of grid points N was determined by the context, typically we took $N = 4000$. No-flux boundary conditions were applied at the ends of the computational domain.

The first consideration is the stability of the travelling waves. Calculations of the temporal eigenvalues reported in (**37**) (for $E = 0$) show that the solutions on the upper branch (Figs 3a, 5a) are stable and those on the lower branch unstable. We did not perform these stability calculations for $E \neq 0$ here. However, in all the numerical integrations that were performed it was only waves on the upper branch that developed in the initial-value problem. This suggests that, in this case as well, the upper branch solutions are temporally stable and the lower branch solutions unstable.

We illustrate the development of the waves in the electric field in Fig. 8 with grey-level plots of w for $f = 2{\cdot}35$ with $E = 0{\cdot}9$ (Fig. 8a) and $E = 2{\cdot}0$ (Fig. 8b). In both cases the electric field is switched on at $t = 6{\cdot}0$ with a polarity indicated in the figure. For the smaller value of E we can see a slight deceleration and thinning of the wave propagating towards the negative electrode. There is a corresponding acceleration and thickening of the wave propagating towards the positive electrode. These changes in speed are relatively small, in line with Fig. 3a. In the stronger field (Fig. 8b) we see the fairly rapid annihilation of the wave propagating towards the negative electrode (here $E > E_m$) with again the acceleration and thickening of the wave propagating towards the positive electrode.

In all the cases that we considered where $E > E_m$, the waves propagating towards the negative electrode were annihilated when the electric field was applied. This suggests that the saddle-node bifurcation at E_m is a strong cut-off value for wave propagation. We next examined the alternative mechanism by which single pulses were terminated at their 'non-existence' curve (see Fig. 5b,c). We illustrate this case in Fig. 8c with a grey-level plot of w for $E = 10{\cdot}0$ and $f = 2{\cdot}32$. For this case we switched the electric field on at $t = 0$ and only a wave propagating towards the positive electrode forms in this strong field. For this value of f the solution terminates at $E = -6{\cdot}0014$ so there is no single pulse that will travel towards the positive electrode. What we do find is the development of a wave train propagating towards the positive electrode. The starting point (local

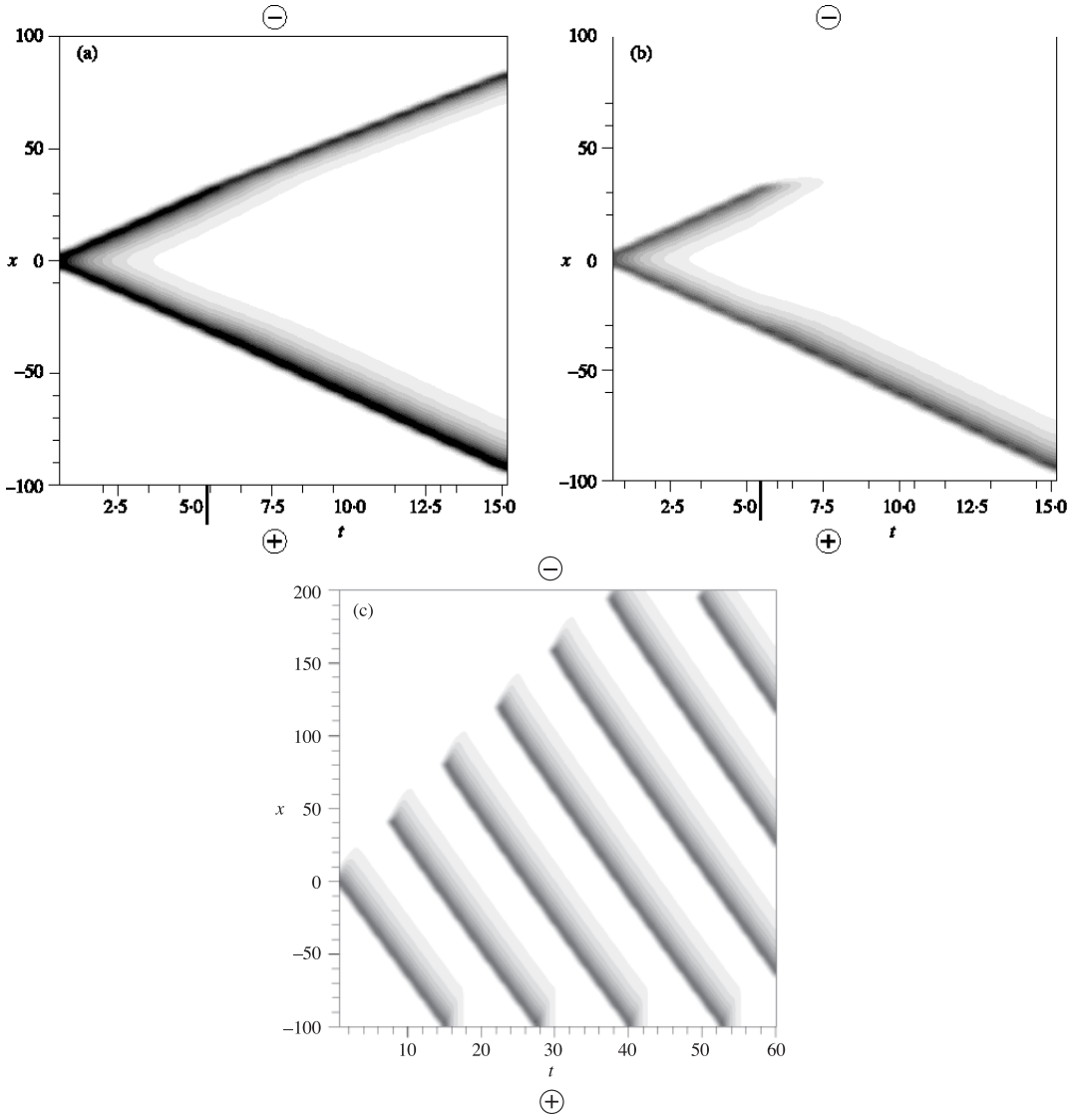

Fig. 8 Grey-level plots of w, obtained from numerical integrations of the initial-value problem (12), (13), for (a) $E = 0{\cdot}9,\ f = 2{\cdot}35$, (b) $E = 2{\cdot}0,\ f = 2{\cdot}35$, electric field switched on at $t = 6{\cdot}0$. (c) $E = 10{\cdot}0,\ f = 2{\cdot}32$, electric field switched on at $t = 0$. The values of the other parameters are $q = 0{\cdot}002,\ \epsilon = 0{\cdot}05,\ D = 1{\cdot}0$. The dark colours correspond to higher concentrations

pacemaker) for these waves moves towards the negative electrode as further waves form in the wave train. A similar situation arises in the case without electric fields when the single pulse solution has terminated at an RH curve (**37**, **39**).

A feature that is observed experimentally is wave reversal (**2**), whereby the direction of propagation of the wave is changed when the polarity of the electric field is reversed. We can

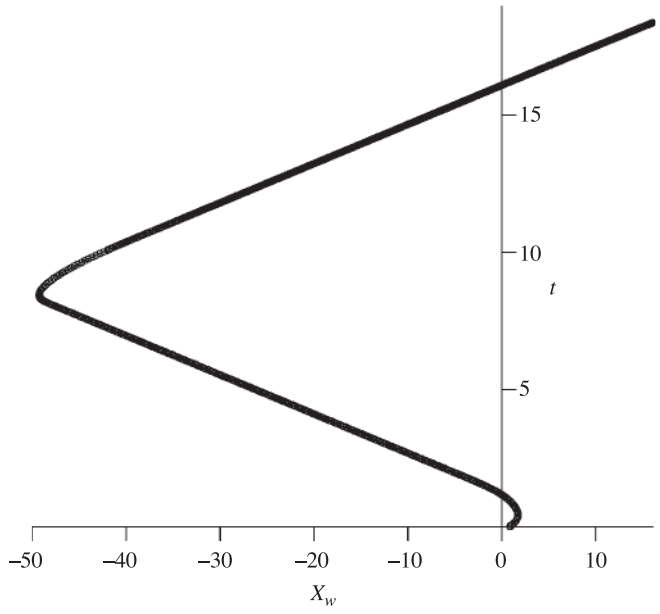

Fig. 9 Wave reversal for $E = 40{\cdot}0$, with a plot of the position of the wave x_w against t. The polarity of the field was switched at $t = 8{\cdot}06$. The values of the other parameters are $f = 2{\cdot}35,\ q = 0{\cdot}002,\ \epsilon = 0{\cdot}05,\ D = 1{\cdot}0$

find this behaviour in our model provided the electric field strengths are relatively high. In this case we start with a high positive field switched on at $t = 0$. In this field only the wave that propagates towards the positive electrode forms. If we then reverse the polarity of the field after this wave has fully developed, its direction of propagation is changed, though it still propagates towards the positive electrode. This is illustrated in Fig. 9 for $E = 40{\cdot}0$ and $f = 2{\cdot}35,\ q = 0{\cdot}002,\ \epsilon = 0{\cdot}05,\ D = 1{\cdot}0$ with a plot of the position of the wave x_w, monitored by the maximum value of u, against t, with the polarity of the field being changed at $t = 8{\cdot}06$. Reversal occurs by the wave first rapidly slowing down and then stopping when the polarity is changed. The u profile starts by reducing in size as the 'tail' of the w profile moves through the wave, with a sharp front appearing towards the new positive electrode. As this profile is being established the u profile starts to grow, reaches its maximum value and then the wave starts propagating in the reversed direction, having the same form and speed as before field reversal.

The numerical integrations show that a high value for E is required for this to happen. For smaller values of E, though still above E_m so that only waves propagating towards the positive electrode form, the wave that does form is annihilated when the polarity is reversed. For the above parameter values we found wave reversal at $E = 30{\cdot}0$ and annihilation with $E = 25{\cdot}0$. The numerical simulations suggest that a necessary condition to see wave reversal is a long recovery region for u and w compared to the excitation region. Thus high field strengths are required (see Fig. 4). This is also borne out when we perform numerical integrations with $D = 2{\cdot}0$. In this case the recovery region is, for the same field strength, longer than for $D = 1{\cdot}0$. In this case we find wave reversal at

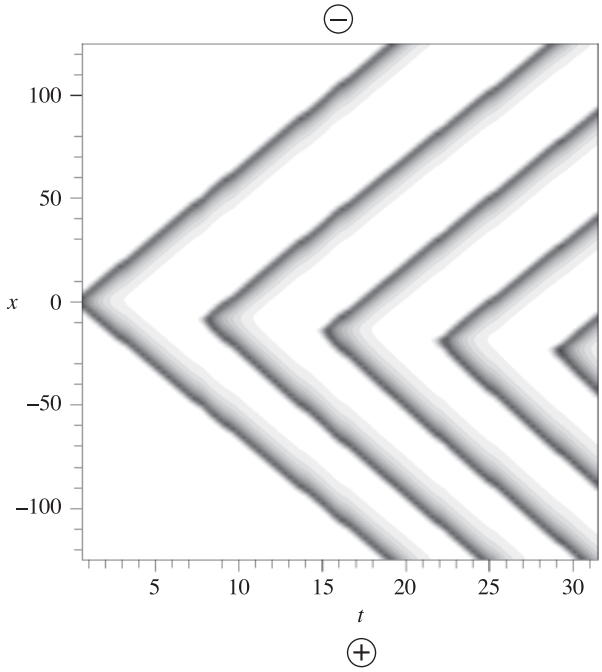

Fig. 10 A grey-level plot of w obtained from numerical integrations of the initial-value problem (12), (13) for $E = 0{\cdot}9,\ D = 0{\cdot}3,\ f = 2{\cdot}25,\ q = 0{\cdot}002,\ \epsilon = 0{\cdot}05$, electric field switched on at $t = 0$, to illustrate the formation of two wave trains. The dark colours correspond to higher concentrations

smaller values of E, with the change from reversal to annihilation occurring between $E = 18{\cdot}0$ and $E = 17{\cdot}5$.

For $D = 0{\cdot}3$ we noted that there were values of f at which waves form only in positive fields (see Fig. 7a). So there are field strengths for which single pulses cannot form in either a positive or a negative field. In this case two wave trains form, one propagating towards the negative electrode and one propagating towards the positive electrode. We illustrate this behaviour in Fig. 10 with a grey-level plot of w for $f = 2{\cdot}25$ and $E = 0{\cdot}9$ (with $q = 0{\cdot}002$, $\epsilon = 0{\cdot}05$) and with the field switched on at $t = 0$. The figure shows the formation of the two wave trains. The wavelength of the wave propagating in the positive direction is greater than that propagating in the negative direction. To accommodate the formation of both wave trains requires the initiation site to move towards the positive electrode as the waves form, as can be seen in the figure.

4. Discussion

We have considered the effect of applying electric fields to waves propagating in the BZ system, which we have described using a two-variable version of the Oregonator model. In this, Br^- is taken to be varying quasi-statically with the two active species $HBrO_2$ and M_{ox}^{3+} (ferriin), the electric field being taken to act only on M_{ox}^{3+}. We have examined the travelling wave equations (18), (19)

for this model in detail, both numerically and by an asymptotic analysis for large negative fields, determining the conditions under which a single pulse wave could exist. We found that there were two ways in which these solutions could be terminated. One was at a saddle-node bifurcation, seen in plots of the wave speed c against the field strength E (Figs 3a, 5a, 7a). This terminating value of E could be positive or negative depending on the values of the other parameters. Numerical integrations of the corresponding initial-value problem showed that waves propagating towards the negative electrode were annihilated when field strengths greater than this were applied. The other mechanism by which single pulses ceased to exist was through a change in sign of the eigenvalues that determine the approach of the solution to the conditions at the rear of the wave. Field strengths at which this occurred were determined by applying the Routh–Hurwitz criteria to equation (21) for these eigenvalues. For field strengths less than this, wave trains were seen in the integrations of the initial-value problem.

We can say a little more about these wave trains in the large $|E|$ limit. They arise in the asymptotic theory when $\alpha > 0$, that is, when $u_s > u_1$, where u_1 is the smaller positive zero of the denominator in equation (31). In this case a singularity develops in the solution, at $Y = -Y_0$ say, in region V, similar to that in region II. This can be removed via regions similar to regions III and IV in the theory for a single pulse. This then returns us to region I, the equation for which now has to be modified to

$$u'' + c_0 u' + \frac{(u-u_1)^2}{\epsilon(u+q)}\left(\frac{f w_1 q}{u_1^2} - u\right) = 0, \quad \text{where } w_1 = \frac{u_1(1-u_1)(u_1+q)}{f(u_1-q)} \tag{44}$$

subject to the matching conditions

$$u \sim u_1 + \frac{\epsilon c_0 (u_1+q)}{(1-u_1)y} + \cdots \text{ as } y \to \infty, \qquad u \to \frac{f w_1 q}{u_1^2} = \frac{(1-u_1)(u_1+q)q}{u_1(u_1-q)} \text{ as } y \to -\infty \tag{45}$$

to complete the periodic nature of the solution in this case. We note that this problem is independent of the parameter f depending only on the parameter q, that $\dfrac{(1-u_1)(u_1+q)q}{u_1(u_1-q)} \simeq 1$ for q small and that the wavelength of the wave train is given to a first approximation by $(\overline{y}_0 + Y_0)|E|$. The parameter ϵ can be scaled out of the problem as before by writing $\tilde{y} = \epsilon^{-1/2} y$, $c_0 = \epsilon^{-1/2}\tilde{c}_0$. A graph of $\tilde{c}_0$ against q obtained from the numerical integration of equations (44), (45) is given in Fig. 11. The figure shows that $\tilde{c}_0$ is relatively insensitive to changes in q and decreases monotonically as q is increased. The values of c_0 obtained for these wave trains are slightly higher than the wave speeds for the single pulses at the parameter values where $\alpha = 0$. For example, for $\epsilon = 0{\cdot}05$, $q = 0{\cdot}002$, $\alpha = 0$ at $f = 2{\cdot}3943$. At this value $c_0 = 7{\cdot}201$ for the wave train compared to $c_0 = 7{\cdot}033$ for the single pulse.

The effect of applying an electric field was to decelerate or annihilate waves propagating towards the negative electrode and to accelerate those propagating towards the positive electrode. The speeds of these latter waves were bounded as the field strength was increased, as was clearly brought out in the asymptotic solution for large $|E|$. This gave a maximum propagation speed in an applied electric field (for given values of the other parameters). This behaviour appears counterintuitive at first sight, and is opposite to what is seen in autocatalytic systems (**28** to **32**), as the ionic species in our model has a positive charge. However, it is the behaviour that is observed experimentally, see (**2**) for example. Also, the effect of the electric field is to steepen the M_{ox}^{3+} profiles in waves

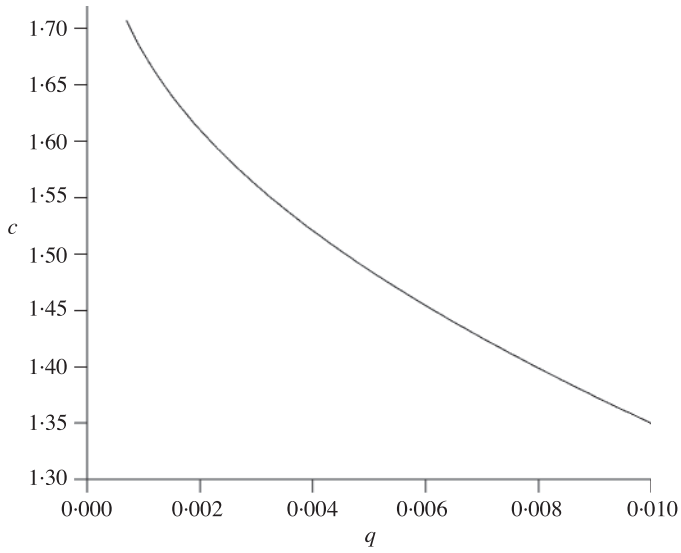

Fig. 11 A plot of the wave speed $\tilde{c}_0$ against q of the wave trains in the large $|E|$ limit, obtained from equations (44), (45), $c_0 = \epsilon^{-1/2}\tilde{c}_0$

propagating towards the negative electrode and to lengthen them when propagating towards the positive electrode (Fig. 4). This is also in agreement with experimental observations (**2**).

Two other features that were observed experimentally are wave reversal and wave splitting (**2** to **5**). We were able to get wave reversal in our model when the polarity of the field was changed, though only at relatively high field strengths. These electric field strengths are very much higher than are needed for annihilation and are probably unrealistic experimentally. We could reduce the field strength needed for reversal by increasing the value of the ratio of the diffusion coeffients D. Again this is not realistic experimentally as $D \simeq 0{\cdot}3$ from values quoted in (**4**). However, a critical difference between wave reversal seen experimentally and in our model is that, in the experiments, it is waves propagating towards the negative electrode that change direction when the polarity is reversed (**2**). In our model, it is the opposite case, it is waves propagating towards the positive electrode that change direction. We were unable to find any wave splitting in our model. We did see wave trains (Figs 8c, 10) but these propagated in the same direction as the initial wave, whereas in wave splitting (**2**, **3**, **5**) the secondary waves propagate in a direction opposite to that of the initial wave.

A critical feature of our model is the reduction from three to two variables via (11). This is a standard approximation that is frequently used in modelling BZ systems and we briefly examine the consequences of following this approach. We concentrate only on the case when $E = 0$ and, taking the same values ($f = 2{\cdot}35$, $\epsilon = 0{\cdot}05$, $q = 0{\cdot}002$, $D_W = 1{\cdot}0$) for both models, we computed the wave profiles from the corresponding initial-value problems for the two-variable (reduced) and three-variable versions of the model; for the three-variable case we took $\epsilon' = 0{\cdot}001$, $D_V = 1{\cdot}0$. If we compare the u and w profiles for the two models, we find that they have comparable initial slopes at the front of the wave. However, both profiles achieve somewhat higher maxima in the

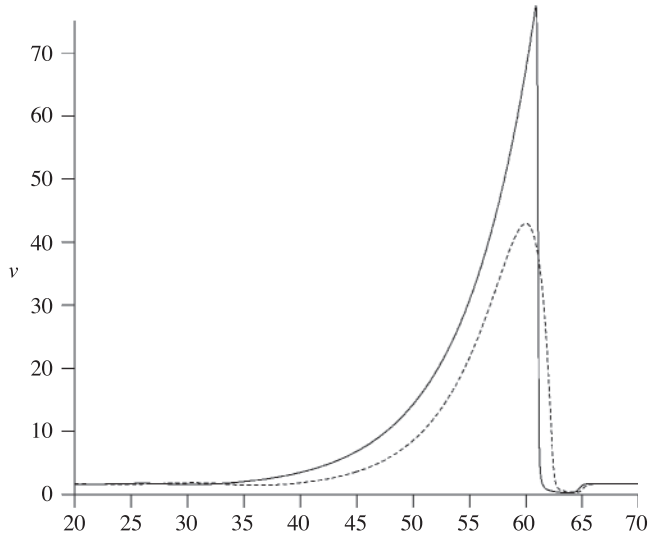

Fig. 12 Plots of v, the dimensionless concentration of Br^-, obtained from the two-variable model (12), (13) (full line) and the three-variable model (6) to (8) (broken line) for $E = 0,\ f = 2{\cdot}35$ and $\epsilon = 0{\cdot}05,\ \epsilon' = 0{\cdot}001,\ q = 0{\cdot}002,\ D_V = D_W = 1{\cdot}0$

two-variable version compared to those in the three-variable case, being about 12 per cent higher. The spread of the waves is comparable in both models. Perhaps the best illustration of the difference between the two models is provided by the v profiles (a dimensionless version of the concentration of Br^-). This is computed directly in the three-variable model and from (11) in the two-variable case. These profiles are shown in Fig. 12. Both profiles have a similar shape, with a fall to small values in the concentration at the front of the wave, achieving a relatively high maximum value before falling to the steady state $v_s = fu_s/(u_s + q)$ at the rear of the wave. However, there are significant differences between the two profiles, the extent of the region of small concentrations at the front of the wave is greater and a considerably higher maximum value is achieved in the two-variable model, about 70 per cent higher, with a correspondingly sharper peak in this profile. The approach to conditions at the rear of the wave is monotone in the two-variable model whereas, in the three-variable model, there are small oscillations in the concentrations at the rear of the wave. Finally, perhaps the most significant difference between the two cases is in the wave speeds. This is somewhat higher, $c \simeq 6{\cdot}1$, for the two-variable model compared to $c \simeq 4{\cdot}8$ in the three-variable case.

The two-variable Oregonator model predicts many of the features seen experimentally when electric fields are applied to BZ systems, giving some qualitative agreement with observations. Thus it is a useful guide for predicting and understanding many of the underlying mechanisms. However, the above considerations, admittedly for only one set of parameter values, suggest that using the quasi-static approximation (11) for the concentration of Br^- is not a particularly viable assumption if more quantitative agreement is required or to obtain some of the fine detail, for example, the wave reversal seen experimentally or wave splitting. These latter features are much more dependent on

the detailed movement of the ionic species, Br^- and M_{ox}^{3+}, in the applied electric fields (**2**, **3**) and could be expected to require the full three-variable version to model them. The strong inhibitory nature of Br^- on the BZ reaction is well established; see (**3**) for example. It is consumed within the excitory part of the reaction and very small concentrations of this species have to be achieved before the reaction can proceed further (**40**). Thus the detailed migration of Br^- within the electric field, which is described only loosely by the two-variable model, can have a strong controlling influence on the nature of wave propagation.

From equations (6) to (8) it might be thought that the ratio $\epsilon'/\epsilon = 2k_4/k_2$ would be a better measure of the validity of the quasi-static approximation (11) rather than just ϵ'. Our results have $\epsilon'/\epsilon = 0{\cdot}02$ and the differences we found between the two cases are perhaps greater than might be expected with this ratio. One point to mention in favour of using the two-variable model is that the time step needed to obtain our results for the three-variable model was $\Delta t = 0{\cdot}001$, making any numerical search of the three-variable model a much lengthier proposition.

Acknowledgements

The authors wish to thank Hana Ševčíková for helpful discussions. We also wish to acknowledge the suport of the ESF Programme REACTOR and IZK wishes to thank ORS and the University of Leeds for financial support.

References

1. H. Sevcikova and M. Marek, Chemical waves in electric field, *Physica* D **9** (1983) 140–156.
2. ——, —— and S. C. Muller, The reversal and splitting of waves in an excitable medium caused by an electric field, *Science* **257** (1992) 951–954.
3. J. Kosek, H. Sevcikova and M. Marek, Splitting of excitable pulse waves, *J. Phys. Chem.* **99** (1995) 6889–6896.
4. H. Sevcikova, I. Schreiber and M. Marek, Dynamics of oxidation Belousov–Zhabotinsky waves in an electric field, *ibid.* **100** (1996) 19153–19164.
5. ——, J. Kosek and M. Marek, Splitting of 2D waves of excitation in a direct current electric field, *ibid.* **100** (1996) 1666–1675.
6. S. C. Muller, O. Steinbock and J. Schutze, Autonomous pacemaker of chemical waves created by spiral annihilation, *Physica* A **188** (1992) 47–54.
7. K. I. Agladze and P. DeKepper, Influence of electric field on rotating spiral waves in the Belousov–Zhabotinsky reaction, *J. Phys. Chem.* **96** (1992) 5239–5242.
8. O. Steinbock, J. Schutze and S. C. Muller, Electric-field-induced drift and deformation of spiral waves in an excitable medium, *Phys. Rev. Letters* **68** (1992) 248–251.
9. V. Perez-Munuzuri, R. Aliev, B. Vasiev and V. I. Krinsky, Electric current control of spiral wave dynamics, *Physica* D **56** (1992) 229–234.
10. A. P. Munuzuri, M. Gomez-Gesteira, V. Perez-Munuzuri, V. I. Krinsky and V. Perez-Villar, Parametric response of a vortex in an active medium, *Phys. Rev.* E **50** (1994) 4258–4261.
11. J. J. Taboada, A. P. Munuzuri, V. Perez-Munuzuri, M. Gomez-Gesteira and V. Perez-Villar, Spiral break up induced by an electric current in a Belousov–Zhabotinsky medium, *Chaos* **4** (1994) 519–524.
12. B. Schmidt and S. C. Muller, Forced parallel drift of spiral waves in the Belousov–Zhabotinsky reaction, *Phys. Rev.* E **55** (1997) 4390–4393.

13. R. J. Field, E. Koros and R. M. Noyes, Oscillations in chemical systems. II. Thorough analysis of temporal oscillation in the bromate–cerium–malonic acid system, *J. Amer. Chem. Soc.* **94** (1972) 8649–8664.
14. —— and R. M. Noyes, Oscillations in chemical systems. IV. Limit cycle behaviour in a model of a real chemical reaction, *J. Chem. Phys.* **60** (1974) 1877–1884.
15. J. J. Tyson, Oscillations, bistability and echo waves in models of the Belousov–Zhabotinskii reaction, *Ann. NY Acad. Sci.* **316** (1979) 279–295.
16. ——, Scaling and reducing the Field–Koros–Noyes mechanism of the Belousov–Zhabotinskii reaction, *J. Phys. Chem.* **86** (1982) 3006–3012.
17. —— and P. C. Fife, Target patterns in a realistic model of the Belousov–Zhabotinskii reaction, *J. Chem. Phys.* **73** (1980) 2224–2237.
18. R. Toth, A. Papp, V. Gaspar, J. H. Merkin, S. K. Scott and A. F. Taylor, Flow-driven instabilities in the Belousov–Zhabotinsky reaction: modelling and experiment, *Phys. Chem. Chem. Phys.* **3** (2001) 957–964.
19. J. R. Bamforth, R. Toth, V. Gaspar and S. K. Scott, Scaling and dynamics of 'flow distributed oscillation patterns'in the Belousov–Zhabotinsky reaction, *ibid.* **4** (2002) 1299–1306.
20. ——, J. H. Merkin, S. K. Scott, R. Toth and V. Gaspar, Flow-distributed patterns in the Oregonator model, *ibid.* **3** (2001) 1435–1438.
21. S. Kadar, J. Wang and K. Showalter, Noise-supported travelling waves in sub-excitable media, *Nature* **391** (1998) 770–772.
22. I. Sendina-Nadal, E. Mihaliuk, J. Wang, V. Perez-Munuzuri and K. Showalter, Wave propagation in subexcitable media with periodically modulated excitability, *Phys. Rev. Letters* **86** (2001) 1646–1649.
23. E. Mihaliuk, T. Sakurai, F. Chirila and K. Showalter, Experimental and theoretical studies of feedback stabilization of propagating wave segments, *Faraday Discussions* **120** (2001) 383–394.
24. S. Schmidt and P. Ortoleva, A new chemical wave equation for ionic systems, *J. Chem. Phys.* **71** (1979) 1010–1015.
25. —— and ——, Multiple waves induced by applied electric field, *ibid.* **67** (1977) 3771–3776.
26. —— and ——, Electric field effects on propagating BZ waves: predictions of an Oregonator and new pulse supporting models, *ibid.* **74** (1981) 4488–4499.
27. P. Ortoleva, Chemical wave–electric field interaction phenomena, *Physica* D **26** (1987) 67–84.
28. D. Snita, H. Sevcikova, M. Marek and J. H. Merkin, Ionic autocatalytic reaction fronts in electric fields, *J. Phys. Chem.* **100** (1996) 18740–18748.
29. ——, ——, —— and ——, Travelling waves in an ionic autocatalytic chemical system with an imposed electric field, *Proc. R. Soc.* A **453** (1997) 2325–2351.
30. ——, ——, J. Lindner, M. Marek and J. H. Merkin, Capillary electrophoresis with chemical reation, *J. Chem. Soc. Faraday Trans.* **94** (1998) 213–222.
31. L. Forstova, H. Sevcikova, M. Marek and J. H. Merkin, Electric field effects on selectivity of reactions within propagating reaction fronts, *Chem. Engng Sci.* **55** (2000) 233–243.
32. ——, ——, —— and ——, Influence of external electric fields on reaction fronts in the iodate–arsenous acid system, *J. Phys. Chem.* A **104** (2000) 9136–9143.
33. J. Mosquera, M. Gomez-Gesteira, V. Perez-Munuzuri, A. P. Munuzuri and V. Perez-Villar, Electric field influence on travelling wave propagation and stationary pattern formation, *J. Bifurcation and Chaos* **5** (1995) 797–807.
34. J. H. Merkin, H. Sevcikova, D. Snita and M. Marek, The effects of an electric field on an

autocatalytic ionic reaction in a system with high ionic strength, *IMA J. Appl. Math.* **60** (1998) 1–31.

35. B. D. Hassard, N. D. Kazarinoff and Y. H. Wan, *Theory and Applications of the Hopf Bifurcation* (Cambridge University Press, Cambridge 1980).

36. J. D. Murray, *Mathematical Biology* (Springer, Berlin 1990).

37. I. Z. Kiss, J. H. Merkin, S. K. Scott and P. L. Simon, Travelling waves in the Oregonator model for the BZ reaction, *Phys. Chem. Chem. Phys.* **5** (2003) 5448–5453.

38. H. Jeffreys and B. S. Jeffreys, *Methods of Mathematical Physics* (Cambridge University Press, Cambridge 1962).

39. P. L. Simon, I. Z. Kiss, J. H. Merkin and S. K. Scott, Wave trains in the Oregonator model for the BZ reaction, in preparation.

40. J. H. Merkin, A. J. Poole, S. K. Scott, J. D. B. Smith and B. W. Thompson, Analysis of the bromate–ferroin clock reaction, *J. Math. Chem.* **19** (1996) 15–32.